catalysts

MDPI

Article

Visible Light Photodegradation of Glyphosate and Methylene Blue Using Defect-Modified Graphitic Carbon Nitride Decorated with Ag/TiO_2

Khalid Aziz [1], Asma Naz [1,*], Suryyia Manzoor [1], Muhammad Imran Khan [2], Abdallah Shanableh [2] and Javier Fernandez Garcia [3,4,*]

[1] Institute of Chemical Sciences, Bahauddin Zakariya University, Multan 60800, Pakistan
[2] Research Institute of Sciences and Engineering (RISE), University of Sharjah, Sharjah 27272, United Arab Emirates
[3] IQS-School of Engineering, Universitat Ramon Llull, Via Augusta 390, 08017 Barcelona, Spain
[4] Warwick Manufacturing Group, Coventry CV4 7AL, UK
* Correspondence: asmanaz@bzu.edu.pk (A.N.); javier.fernandez@iqs.url.edu (J.F.G.)

Abstract: The presence of various organic pollutants in surface and ground waters has raised serious environmental threats across the world. In the present work, the solvothermal process was applied to prepare a ternary composite of barium defect-modified graphitic carbon nitride (DM g. C_3N_4) decorated with silver and titanium oxide for the photocatalytic removal of dyes and pesticides in visible light. Methylene blue (MB) and glyphosate were targeted pollutants. Enhanced structural defects in the carbon nitride framework were reported and characterized by using FTIR, SEM, EDS, XRD, and UV/Visible spectroscopy. Various analytical techniques confirmed the proficient coating of titanium oxide and silver on the surface of DM g. C_3N_4. The photocatalytic efficiency of synthesized materials for the degradation of persistent organic pollutants and various parameters such as the effect of pH, catalytic dosage, the concentration of pollutant, reusability of the catalyst, etc., were estimated by using UV/Visible spectroscopy. Batch experiments were performed to estimate the degradation efficiency and other parameters by using an absorption study. A scavenger analysis confirmed hydroxyl radicals as the main reactive species for the degradation of various pollutants. The results confirm that the ternary composite of barium DM g. C_3N_4 showed an increased response in the visible region, greater stability, and excellent photocatalytic efficiency toward the degradation of the organic compounds. The results confirm that the maximum degradation of the said organic pollutants occurs in 105 min.

Keywords: defect-modified graphitic carbon nitride; glyphosate; methylene blue; photocatalytic degradation

check for updates

Citation: Aziz, K.; Naz, A.; Manzoor, S.; Khan, M.I.; Shanableh, A.; Fernandez Garcia, J. Visible Light Photodegradation of Glyphosate and Methylene Blue Using Defect-Modified Graphitic Carbon Nitride Decorated with Ag/TiO_2. *Catalysts* **2023**, *13*, 1087. https://doi.org/10.3390/catal13071087

Academic Editor: Hongxing Dai

Received: 13 February 2023
Revised: 21 March 2023
Accepted: 6 July 2023
Published: 11 July 2023

Copyright: © 2023 by the authors. Licensee MDPI, Basel, Switzerland. This article is an open access article distributed under the terms and conditions of the Creative Commons Attribution (CC BY) license (https://creativecommons.org/licenses/by/4.0/).

1. Introduction

Pure and clean water is not just a fundamental need for humans, but for all living organisms. Countless deaths among species are reported regularly as a result of diseases caused by contaminated water [1]. One of the most threatening problems of our ecosystem is waste materials that cause water pollution. With the growing needs of humanity, industrialization is increasing day by day. As a result, the concentration of toxic contaminants is rapidly growing in the air, land, and water [2]. Most organic and inorganic effluents pose a serious threat to our ecosystem through the contamination of water. Pesticides, dyes, plastics, pharmaceuticals, and personal care products are the most common sources of water contamination. Industrial and domestic waste is mainly discharged into the water reservoirs without pretreatment [3].

Dyes play a vital role in human life because they are used in various fields as coloring agents. Although dyes are essential to our lives, they also pose significant threats to aquatic life because they are one of the main causes of water contamination [4]. When these

dyes enter biological systems, they are converted into toxic carcinogens through microbial degradation. Azo dyes contain the R-N=N-R group and they are considered an almost non-degradable class of compounds. They are widely applied as coloring agents in various industries like textile, food, leather, and pharmaceutical products [5].

Methylene blue (MB) is a versatile aromatic compound applied in various fields. The German chemist Heinrich Caro manufactured methylene blue for the first time. Since then, it has been abundantly used in medical facilities, various chemicals, the pharmaceutical industry, the textile and leather industry, etc. MB is the first ever synthetic compound to be applied as an antiseptic in clinical therapy. It is also used as a redox indicator. The global market value of MB dye was estimated to be more than USD six million in 2020. It is further anticipated to reach USD nine million at the end of 2025 [6].

Another class of organic compounds that cause hazardous effects on aquatic life are pesticides that are applied to prevent pests, insects, and unwanted plants from destroying crops [7]. Glyphosate is a white crystalline solid herbicide from the organophosphate group. The importance of glyphosate as an herbicide was discovered by John E. Franz in 1970. Monsanto used it in agriculture for the first time in 1974. Since then, it has become the most widely used pesticide in the world as a weed killer, especially for broad-leaf weeds. In the last decade, more than two billion tons of glyphosate was used worldwide. As glyphosate and its formulations are widely applied in the world, there is an increasing concern about its adverse effect on the environment, aquatic life, and human beings [8]. According to a report, only 3–5% of applied pesticides reach their actual target, and the remaining portion of them leaches to the water sources, causing threats to aquatic life [9]. These waste effluents should be treated properly before releasing them into water resources. Although legislation for protecting the environment is present worldwide, the lack of strict implementation of laws in developing and poor countries is a major problem. Moreover, many effluents are not removed or they are degraded via simple conventional methods of remediation [10].

Considering the hazardous effects of persistent organic effluents on the ecosystem, it is important to find efficient methods for the removal of these pollutants. Several conventional methods like physical absorption, treatment via chemical methods, and biological ways of remediation, are applied for the treatment of different pollutants. These traditional methods are based on filtration, chemical oxidation, filtration through membrane, crystallization, sedimentation, etc. These conventional methods show certain limits due to less removal efficiency and a higher cost [11]. Considering the limitations of conventional methods, it is necessary to design such proactive methods that may provide excellent results for the degradation of persistent effluents into simple and environmentally friendly by-products such as water, carbon dioxide, etc. [12].

Nanotechnology is widely applied in various fields, as nanoparticles' mechanical, electrical, and optical properties can easily be controlled by a large surface area, composition, and symmetry [13]. The nanoparticles' required functional properties and morphology can be achieved via controlled synthesis [14]. Various nanoparticles are applied for remediation purposes because they are highly efficient absorbents due to their good reactivity and high mobility in solutions, and their active surface area increases with the decreasing particle size [15]. These nanomaterials include various nitrides, sulfides, oxides, nitrates, aluminates, ferrites, etc., and their composites with various other metals and nonmetals.

In recent times, environmental remediation has widely regarded photocatalysis as a promising and effective method. This method is particularly applied to the degradation of persistent organic pollutants such as dyes, pesticides, pharmaceutical waste, personal care products waste, etc. [16]. Photocatalysis is favored over other remediation techniques because it is inexpensive, powerful, eco-friendly, easy to manipulate with different operational parameters, and can completely mineralize hazardous pollutants [17]. During photocatalysis, organic pollutants are transformed into simple minerals, carbon dioxide, water, etc. [18]. Currently, semiconductor nanomaterials are widely used for the photodegradation of organic pollutants. Photocatalysis involves the absorption of photons to activate materials.

The particle size and morphology of the synthesized material play important roles in controlling and modifying the properties required for a specific application [19].

Recently, polymeric graphitic carbon nitride (g. C_3N_4) has attracted considerable attention due to its eco-friendly nature and lower cost. Additionally, it is metal-free and has a large surface area that is beneficial for more reactive sites. Carbon nitride nanoparticles can be applied in a variety of areas, such as environmental remediation, energy storage, production, etc. [20]. However, certain limitations and challenges are associated with using pure carbon nitride for environmental remediation. These challenges include a higher recombination rate, the inefficiency of the material to work in the visible region, and the smaller surface area. The desired properties of pristine g. C_3N_4 can be improved by tailoring and modifying the material. Introducing barium defects to g. C_3N_4 may improve the surface area, resulting in a greater photocatalytic efficiency [21]. The introduction of barium defects also decreases the recombination process of electrons and holes. The modification of g. C_3N_4 may be carried out by introducing barium or calcium carbonates and nitrates [22]. Modifications in the electronic framework and band gap of pristine or modified graphitic carbon nitride can be obtained by doping with different metals, nonmetals, or metal oxides. Most transition metals are widely used for this purpose, while halogens, nitrogen oxygen, sulfur, phosphorus, etc., are nonmetals that are generally used for modification purposes.

Titanium oxide is an efficient metal oxide for degradation because of its low cost, better efficiency, and eco-friendly nature, while because of the wide band gap and the lower efficiency in the visible region, the use of bare titanium oxide is limited. The composite containing titanium oxide with defect-modified carbon nitride can dramatically increase the degradation efficiency, increase the response of the visible region, and decrease the recombination of holes and electrons [23].

The introduction of transition metals like silver in this binary composite may further improve the surface area. In addition, the introduction of metal may also increase the electron mobility and the conductivity of the material. A decreased recombination rate and larger surface area are obtained by the heterojunction of g. C_3N_4. These properties predict a higher degradation efficiency of persistent organic compounds. The doping of g. C_3N_4 with metal or metal oxide promotes a fast charge transfer, greater degradation efficiency, better surface area, interfacial properties, and greater material stability. Thus, by realizing this fact, it is possible to apply the preparation of ultrafine carbon nitride composite decorated with metal or metal oxide for the effective removal of organic pollutants [24].

In our study, barium defect-modified carbon nitride (DM g. C_3N_4) is decorated with Ag and TiO_2. The synthesized ternary composite produced excellent results for the catalytic degradation of dyes and pesticides.

2. Results and Discussion

2.1. Structural Analysis

The FTIR results for the various prepared materials are shown in Figure 1. Various absorption peaks in the range from 500 cm^{-1} to 2000 cm^{-1} were found for g. C_3N_4. A peak at 800 cm^{-1} was associated with bending vibrations of the heptazine ring of g. C_3N_4. Peaks in the range of 1240 cm^{-1} to 1650 cm^{-1} were assigned to the stretching vibrations occurring in the heterocycle of CN. The bands observed around 3700–3800 cm^{-1} were assigned to the stretching vibrations of the terminal NH_2 or NH groups and to the absorbed water that was present on the defects' site of the aromatic ring. It was noted that the specific peak of g. C_3N_4 was persistent in all the synthesized materials. These persistent peaks confirmed that no major changes in the structural framework of the carbon nitride occurred when silver and titanium oxide were deposited on the carbon nitride.

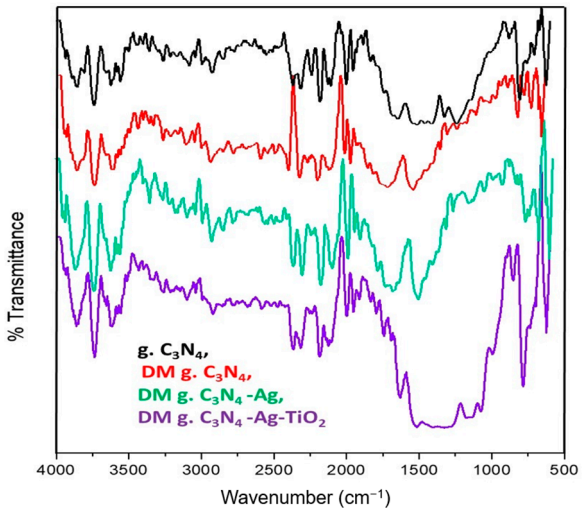


Figure 1. FTIR of g. C_3N_4, DM g. C_3N_4, DM g. C_3N_4-Ag, and DM g. C_3N_4-Ag-TiO_2.

2.2. XRD

The XRD results for the synthesized nanoparticles are shown in Figure 2. The phase structures of the synthesized materials determined via XRD confirmed a distinct peak at 27.4° for pristine g. C_3N_4. This peak was indexed as (002). The peak of g. C_3N_4 was found to be persistent in all the prepared materials. The presence of the characteristic peak of g. C_3N_4 in all samples confirmed that the structure of the base material remained intact after modification. The intensity of the g. C_3N_4 peak became smaller in the silver-decorated carbon nitride and was further decreased by introducing silver and titanium oxide. The well crystalline anatase phase of titanium oxide was found with characteristic peaks at 25°, 54°, and 64°. The characteristic peaks of titanium oxide were indexed as (101), (211), and (220), respectively. The face-centered cubic silver showed characteristic peaks at 38°, 44°, 48°, and 77°. Peaks of silver were indexed as (111), (200), (220), and (311), respectively. These results confirm the efficient packing of Ag and TiO_2 on the surface of DM g. C_3N_4. The average particle sizes (nanometer) of g. C_3N_4, DM g. C_3N_4, DM g. C_3N_4-Ag, and DM g. C_3N_4-Ag-TiO_2 calculated using the Debye–Scherrer formula were 25.12, 27.3, 44.12, and 25.12, respectively.

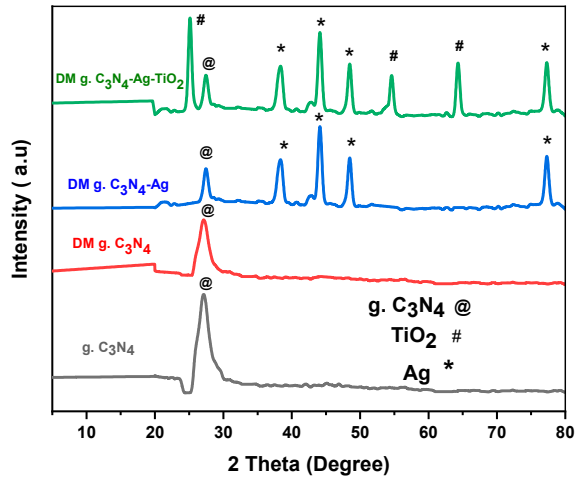


Figure 2. XRD of g. C_3N_4, DM g. C_3N_4, DM g. C_3N_4-Ag, and DM g. C_3N_4-Ag-TiO_2.

2.3. Morphological Analysis

The SEM images of pristine g. C_3N_4, DM g. C_3N_4, DM g. C_3N_4-Ag, and DM g. C_3N_4-Ag-TiO_2 are presented in Figure 3a–h, respectively. These results confirm the template formation by tiny nanodots on the surface of g. C_3N_4. The barium defect-modified graphitic

carbon nitride indicated two-dimensional lamellar structures that have layers and pleats. The slightly porous and sponge-like structure of the nanoparticles predicted a network structure with enhanced catalytic properties. The structural layers of the graphitic carbon nitride started to decrease with the addition of silver and titanium oxide. This decrease was also confirmed by the XRD analysis, where the intensity of the peaks of the g. C_3N_4 decreased with the introduction of silver and titanium oxide. The DM g. C_3N_4-Ag and DM g. C_3N_4-TiO_2-Ag did not show a significant presence of silver nanoparticles. This confirms the uniform and single-path growth of nano-sized silver nanoparticles on the surface of g. C_3N_4. The ternary composite DM g. C_3N_4-TiO_2-Ag indicated two-dimensional hierarchical structures as a template of the composite. The presence of uniform plate-like structures with pores and tube-like structures confirmed the successful synthesis of the ternary composite [25].

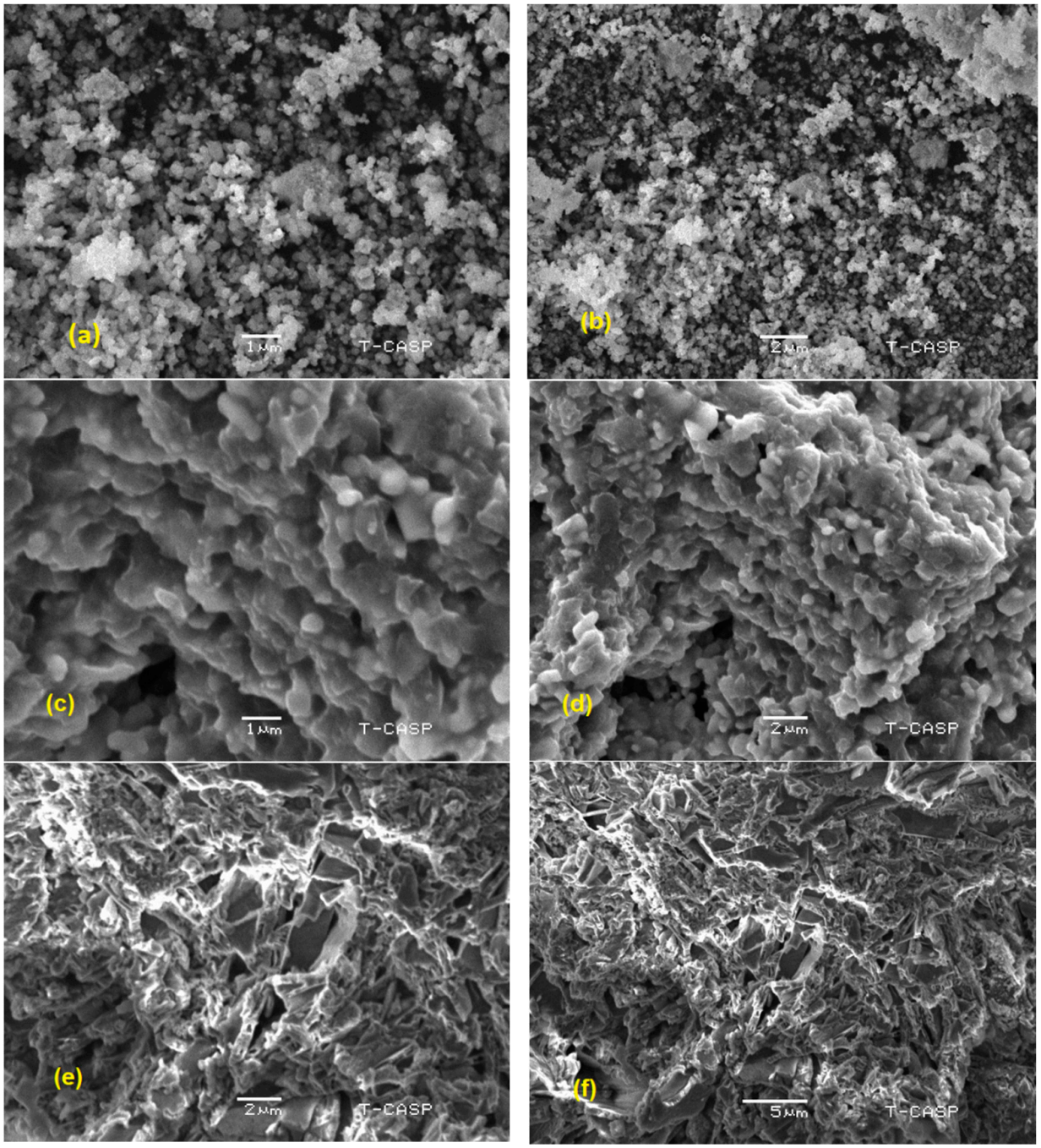


Figure 3. *Cont.*

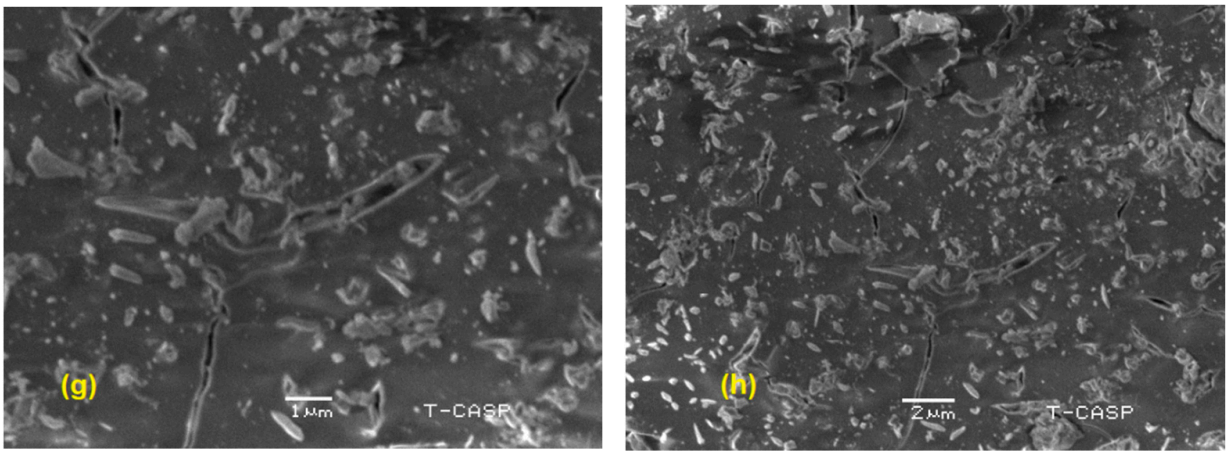
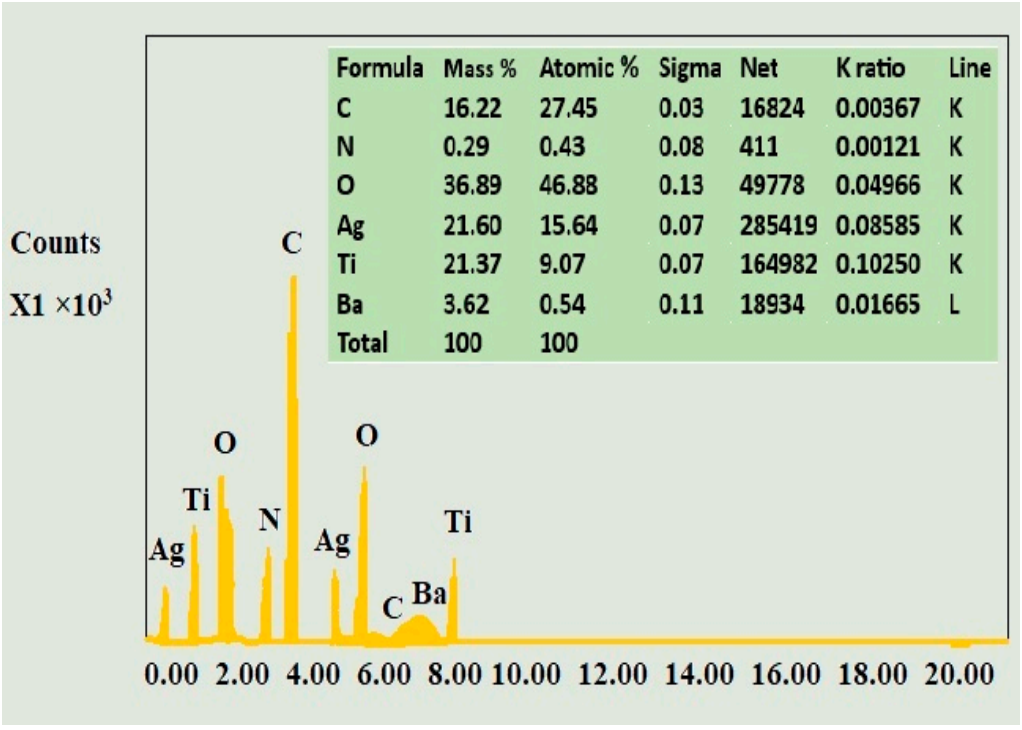


Figure 3. SEM images of (**a**,**b**) g. C_3N_4, (**c**,**d**) DM g. C_3N_4, (**e**,**f**) DM g. C_3N_4-Ag, (**g**,**h**) DM g. C_3N_4-Ag-TiO_2.

2.4. Energy Dispersive X-ray Spectroscopy (EDS) Analysis

The EDS spectrum of the ternary composite is shown in Figure 4. This confirms the presence of carbon, nitrogen, oxygen, silver, titanium, and barium with atomic percentages of 27.45, 0.43, 36.89, 21.60, 21.37, and 3.62, respectively. The presence of noticeable peaks of the required elements in the EDS spectrum of the composite confirmed the efficient coating of titanium oxide and silver on the surface of barium defect-modified graphitic carbon nitride.



Formula	Mass %	Atomic %	Sigma	Net	K ratio	Line
C	16.22	27.45	0.03	16824	0.00367	K
N	0.29	0.43	0.08	411	0.00121	K
O	36.89	46.88	0.13	49778	0.04966	K
Ag	21.60	15.64	0.07	285419	0.08585	K
Ti	21.37	9.07	0.07	164982	0.10250	K
Ba	3.62	0.54	0.11	18934	0.01665	L
Total	100	100				

Figure 4. EDS spectrum of DM g. C_3N_4-Ag-TiO_2.

2.5. Optical Properties of Synthesized Nanoparticles

Characteristic peaks were observed in the visible region for all the synthesized materials. Pure g. C_3N_4 showed an absorption peak at a 420 nm wavelength. A considerable redshift was observed when silver and titanium oxide were introduced to the base material. The enhanced rate of formation of electron and hole pairs at the surface of the photocatalyst was considered to be the major reason for the redshift. The transfer rate of electrons at

the interface also increased with the introduction of silver and titanium oxide, resulting in absorption at a higher wavelength. The Kubelka–Munk function was applied for the determination of the band gap of the synthesized materials [26].

$$(\alpha h\upsilon)^2 = A\ (h\upsilon - E_g) \quad (1)$$

Here, α is the absorption coefficient, υ is the light frequency, A is the proportionality constant, E_g is the band gap energy, and h is Planck's constant.

A graph was plotted by taking $h\upsilon$ on the X-axis and $(\alpha h\upsilon)^2$ on the Y-axis for the determination of the energy band gap. The band gap values were calculated by extrapolating the trending line on the X-axis [26]. The Kubelka–Munk functions for the band gap determination of the various synthesized nanomaterials are shown in Figure 5a–d. By using the Kubelka–Munk function, the calculated band gap values for g. C_3N_4, DM g. C_3N_4, DM g. C_3N_4-Ag, and DM g. C_3N_4-Ag-TiO_2 were 2.72, 2.39, 2.31, and 2.23, respectively.

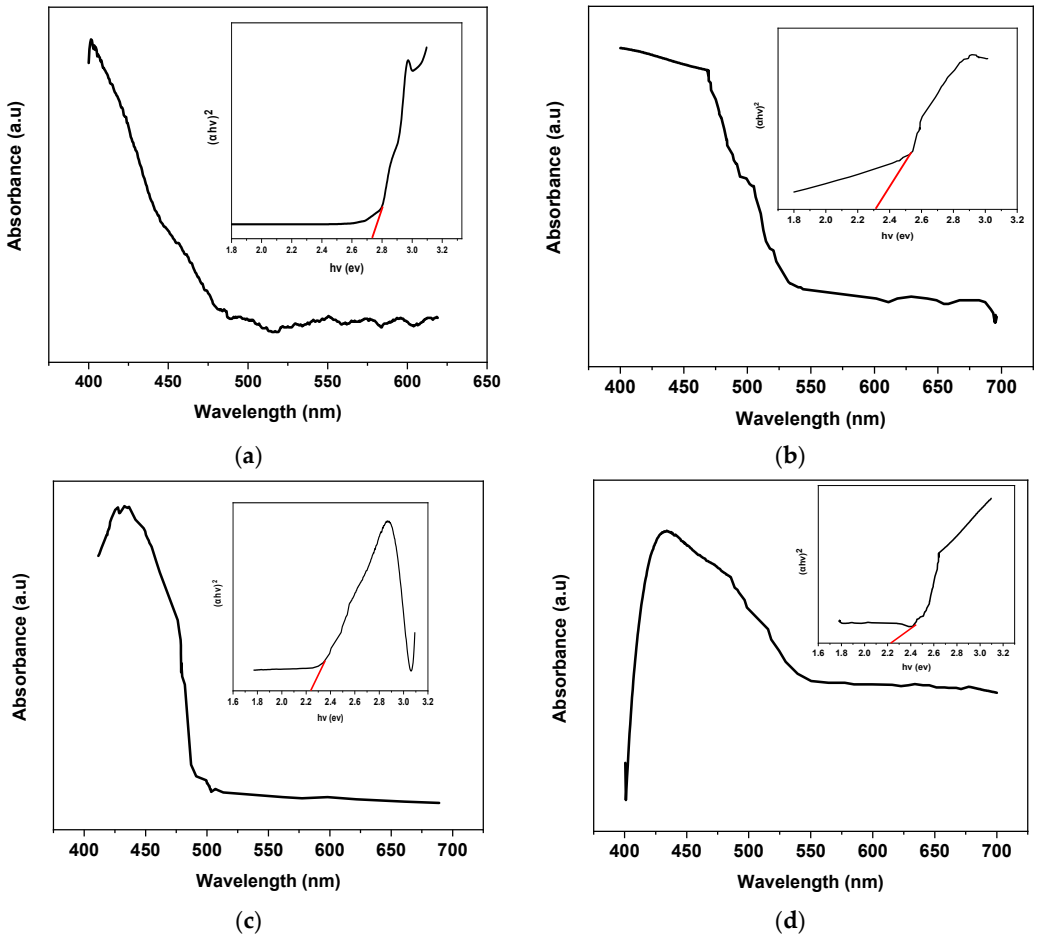


Figure 5. UV/Vis spectrum of nanoparticles and Kubelka–Munk function for BG (inset) (**a**) g. C_3N_4, (**b**) DM g. C_3N_4, (**c**) DM g. C_3N_4-Ag, (**d**) DM g. C_3N_4-Ag-TiO_2.

2.6. Photoluminescence (PL) Spectroscopy

The stability of the nanoparticles depends upon the stability of the generated electrons and holes, which plays a very vital role in the catalytic performance of the prepared materials. A lower recombination rate of electrons and holes provides a lesser intensity of the PL spectrum, confirming the stability of the prepared material. Various prepared materials were subjected to PL. The results provide a strong PL emission spectrum of around 460 nm for g. C_3N_4. The strong peak for g. C_3N_4 indicates that the photogenerated electrons and holes combined immediately. The DM g. C_3N_4, DM g. C_3N_4-Ag, and DM g. C_3N_4-Ag-TiO_2 also show a PL emission peak at around 460 nm. The PL spectrum shows the least emission peak for the DM g. C_3N_4-Ag-TiO_2. A decrease in the peak intensity

indicates a decrease in the recombination rate of the holes and electrons (Figure 6). With the increase in the life of the excited electrons and holes, the stability of the material increases, and the catalytic performance increases. The increase in the photocatalytic activity is also validated by the increase in the degradation efficiency of MB and glyphosate using DM g. C_3N_4-Ag-TiO_2.

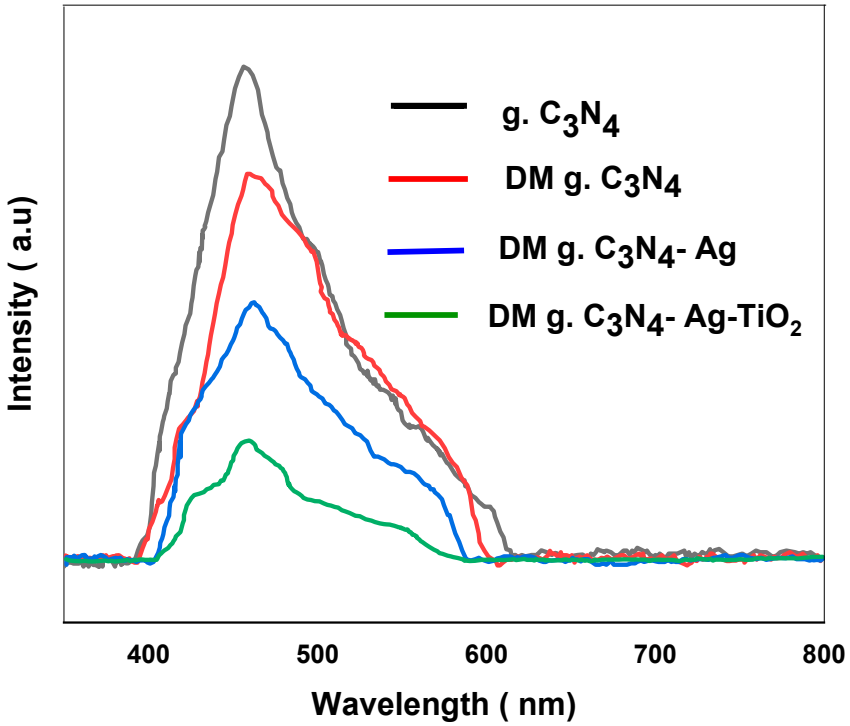


Figure 6. Photoluminescence spectrum of g. C_3N_4, DM g. C_3N_4, DM g. C_3N_4-Ag, DM g. C_3N_4-Ag-TiO_2.

2.7. Photodegradation of MB and Glyphosate

Various synthesized materials were investigated for the photocatalytic removal of targeted pollutants under visible light to evaluate the photocatalytic performance. The results reveal that after 24 h (1440 min) of photolytic degradation, MB and glyphosate only degraded by 5% and 6%, respectively. However, in the presence of photocatalysts (g. C_3N_4, DM g. C_3N_4, DM g. C_3N_4-Ag, DM g. C_3N_4-Ag-TiO_2), MB and glyphosate took only 105 min and caused a higher degradation. The maximum degradation of 96% was achieved by using DM g. C_3N_4-Ag-TiO_2. This confirms that the major degradation of pollutants was due to photocatalytic materials [27]. With time, the absorbance value for MB and glyphosate decreased, indicating a decrease in the concentration of pollutants [28]. The photocatalytic degradation results of methylene blue and glyphosate by using various synthesized nanoparticles are shown in Figure 7a–j. The degradation results for MB and glyphosate by using synthesized materials are listed in Table 1.

Table 1. The photocatalytic efficiency of various nanoparticles for the degradation of MB and glyphosate.

Photocatalyst	Time (min)	MB Degradation (%)	Glyphosate Degradation (%)
Photolytic	1440	5	6
g. C_3N_4	105	57	47
DM g. C_3N_4	105	66	58
DM g. C_3N_4-Ag	105	78	78
DM g. C_3N_4-Ag-TiO_2	105	98	96

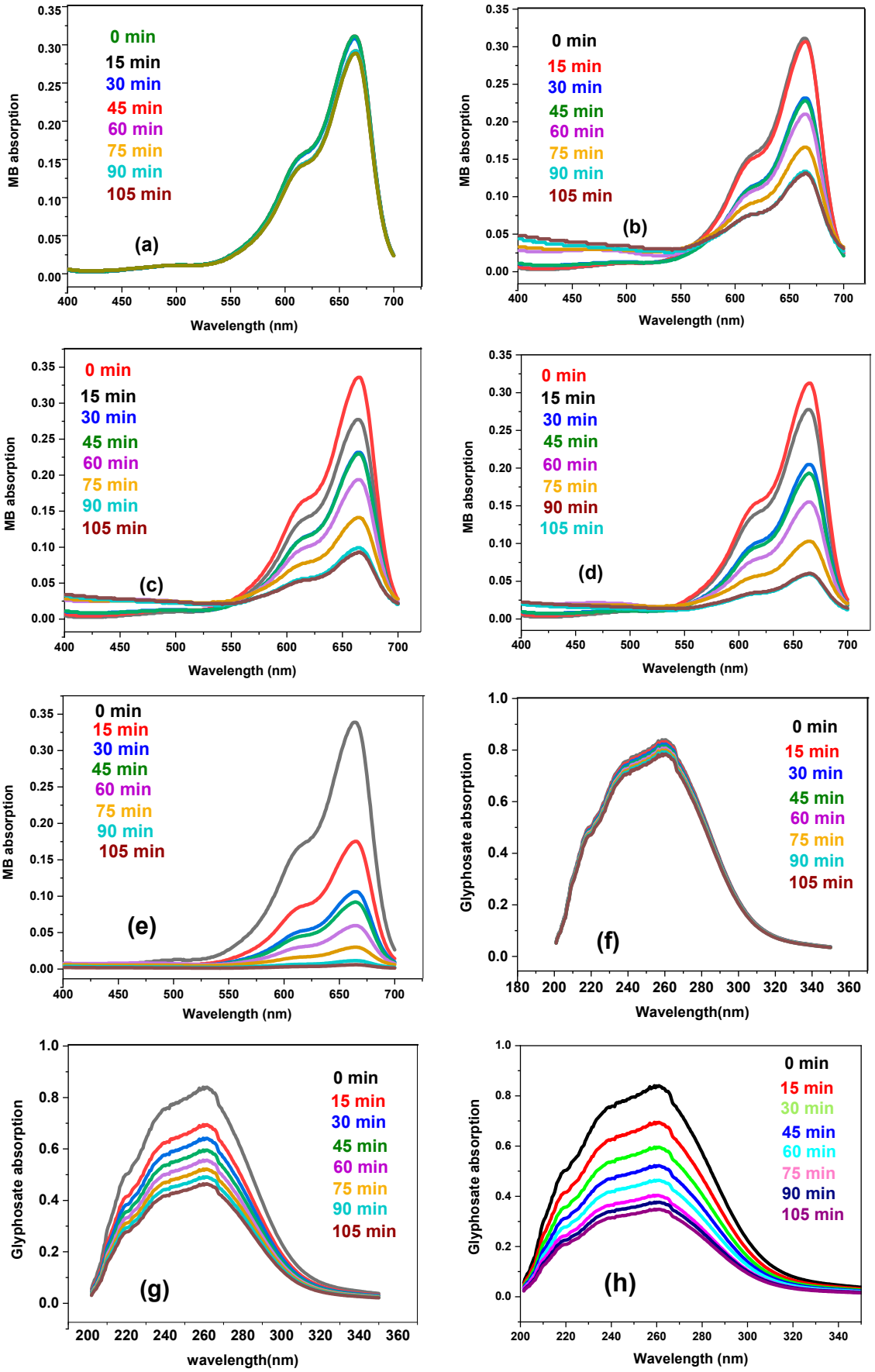


Figure 7. *Cont.*

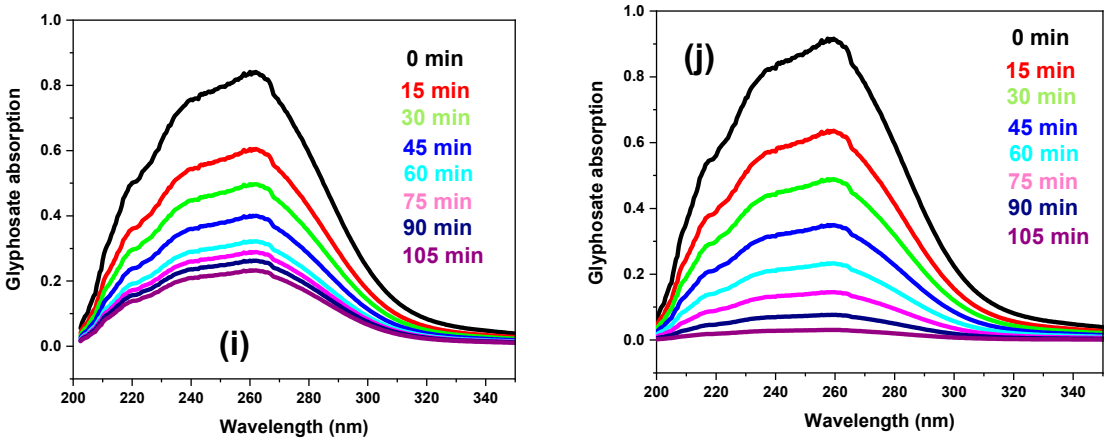


Figure 7. (**a**) Photolytic degradation of MB. (**b**–**e**) Photocatalytic degradation of MB by g. C_3N_4, DM g. C_3N_4, DM g. C_3N_4-Ag, and DM g. C_3N_4-Ag-TiO_2. (**f**) Photolytic degradation of glyphosate. (**g**–**j**) Photocatalytic degradation of glyphosate by g. C_3N_4, DM g. C_3N_4, DM g. C_3N_4-Ag, and DM g. C_3N_4-Ag-TiO_2.

2.8. Scavenger Analysis for Reactive Species and Possible Photocatalytic Mechanism

In the scavenger analysis, the hydroxyl radicals were trapped by isopropyl alcohol (IPA), while the superoxide and holes were trapped by benzoquinone and Na_2-EDTA, respectively. These scavengers were added for trapping reactive species, while the remaining experimental conditions for the photocatalytic degradation of pollutants remained the same. A fixed concentration (2 mM) of scavenger was added with DM g. C_3N_4-Ag-TiO_2 in the pollutant solution, and the absorption spectrum was recorded using a UV/Visible spectrophotometer. As indicated in Figure 8a,b, with the addition of IPA and Na_2-EDTA, a significant drop in the degradation efficiency after 105 min was recorded, which confirms the major role of hydroxyl radicals and holes in the degradation process. The hydroxyl radicals were trapped by the addition of IPA, hence becoming unavailable for the degradation of pollutants. Similarly, the results confirm that the addition of Na_2-EDTA also trapped holes and reduced the generation of hydroxyl radicals. The addition of benzoquinone indicated less effect on the degradation of pollutants. The scavenger analysis confirmed that the photodegradation of dyes and pesticides is mainly due to hydroxyl radicals.

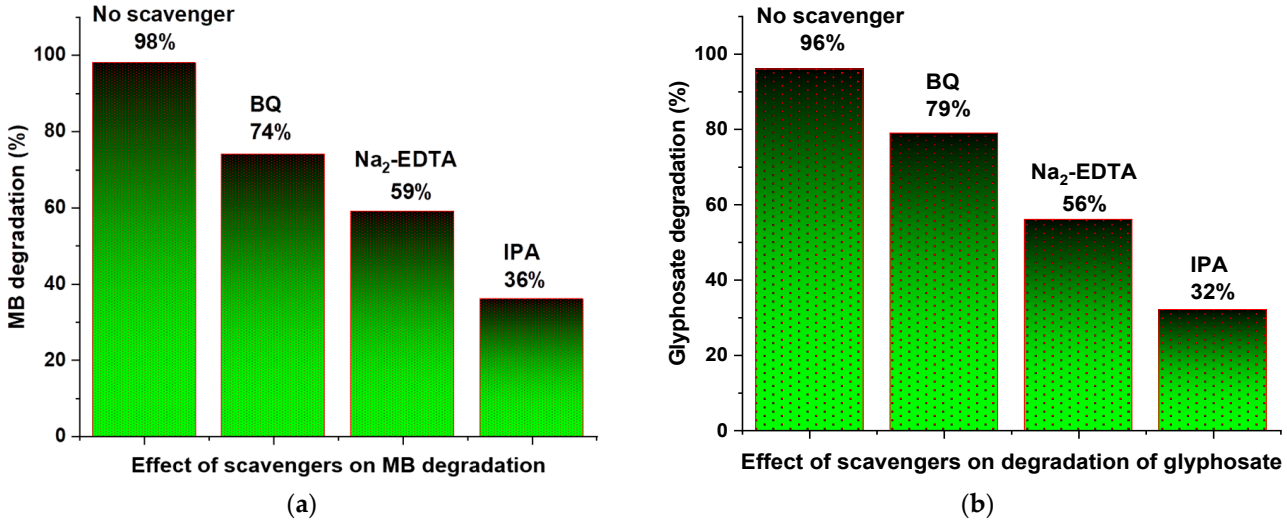


Figure 8. Effect of various scavengers on (**a**) MB and (**b**) glyphosate degradation using DM g. C_3N_4-Ag-TiO_2 after 105 min.

The photocatalytic process can be initiated by shifting electrons from the valence band (VB) to the empty conduction band (CB). This excitation occurs when the amount of energy absorbed by the photon is more than the band gap energy of the material. When an excited electron reaches the conduction band, a vacancy called a hole is produced in the valence band. In this way, holes and electrons are produced simultaneously. Electrons and holes produced by the excitation process are used for the production of hydroxyl radicals, which are primarily applied in the degradation of persistent organic pollutants into simple products, mostly carbon dioxide and water [29]. The possible photocatalytic degradation mechanism is illustrated in Figure 9.

$$\text{DM g. } C_3N_4\text{–Ag} - TiO_2 + h\nu \rightarrow e^- + h^+ \quad (2)$$

$$O_2 + e^- \rightarrow \bullet O_2^- \quad (3)$$

$$h^+ + H_2O \rightarrow H^+ + OH^\bullet \quad (4)$$

$$2h^+ + 2H_2O \rightarrow 2H^+ + H_2O_2 \quad (5)$$

H_2O_2 produces hydroxyl radicals and $\bullet O_2^-$

$$H_2O_2 \rightarrow 2OH^\bullet \quad (6)$$

$$H_2O_2 + e^- \rightarrow OH^- + OH^\bullet \quad (7)$$

$$OH^- + h^+ \rightarrow OH^\bullet \quad (8)$$

$$\bullet O_2^- + H^+ \rightarrow \bullet HO_2 \quad (9)$$

$\bullet HO_2$ produces H_2O_2, which further produces hydroxyl radicals

$$H^+ + \bullet O_2^- + \bullet HO_2 \rightarrow O_2 + H_2O_2 \quad (10)$$

These hydroxyl radicals degrade persistent organic pollutants into less hazardous products, mainly carbon dioxide, water, mineral acids, etc.

$$\bullet OH + \text{MB/Glyphosate} \rightarrow \text{Degradation products(mainly } CO_2 \text{ and } H_2O) \quad (11)$$

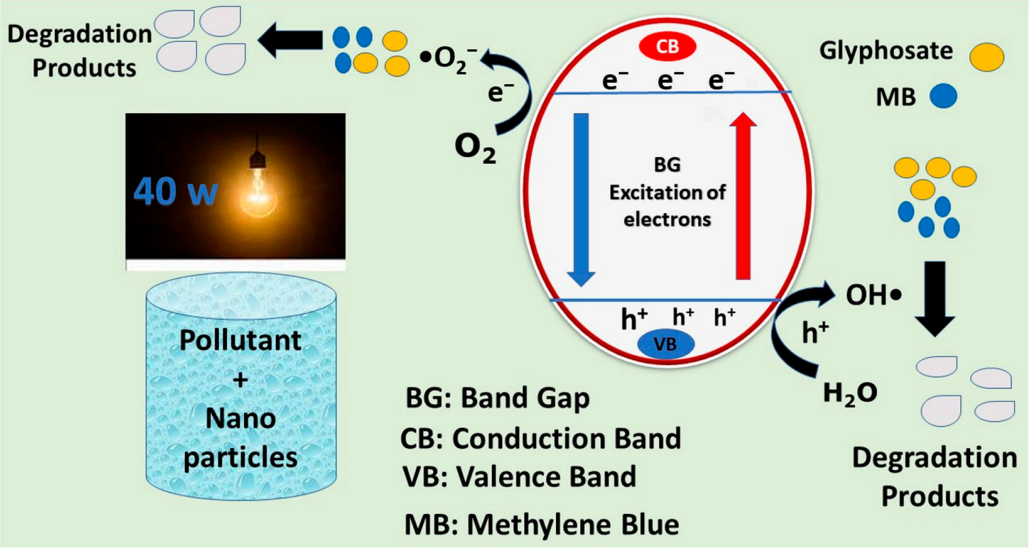


Figure 9. The possible photocatalytic mechanism for the degradation of pollutants by nanoparticles.

2.9. Evaluation of Different Parameters for Pollutant Degradation

2.9.1. Catalytic Dosage

It is important to find the optimum amount of synthesized material to degrade a specific concentration of organic pollutants. The photocatalytic efficiency of DM g. C_3N_4-Ag-TiO_2 for glyphosate and MB degradation was evaluated by varying concentrations of prepared materials, as shown in Figure 10a [30]. For degradation purposes, the concentration of DM g. C_3N_4-Ag-TiO_2 was varied from 10 mg L^{-1} to 200 mg L^{-1}, and the degradation of MB and glyphosate was studied for 105 min. By increasing the concentration of the photocatalyst from 10 mg L^{-1} to 100 mg L^{-1}, the MB degradation efficiency increased from 56% to 97%. The glyphosate degradation also increased from 51% to 95% when the catalyst amount was increased from 10 mg L^{-1} to 200 mg L^{-1}. An increase in the degradation efficiency with an increasing amount of photocatalysts was attributed to the increasing number of produced hydroxyl radicals. When the dosage of the catalyst was further increased from 100 mg L^{-1}, the degradation efficiency of glyphosate and MB started to decrease. A decrease in the degradation efficiency with an increasing catalyst dosage could be due to turbidity. Moreover, with the increasing amount of catalysts, the efficiency of active sites producing free radicals decreased due to a decrease in the light absorption [31].

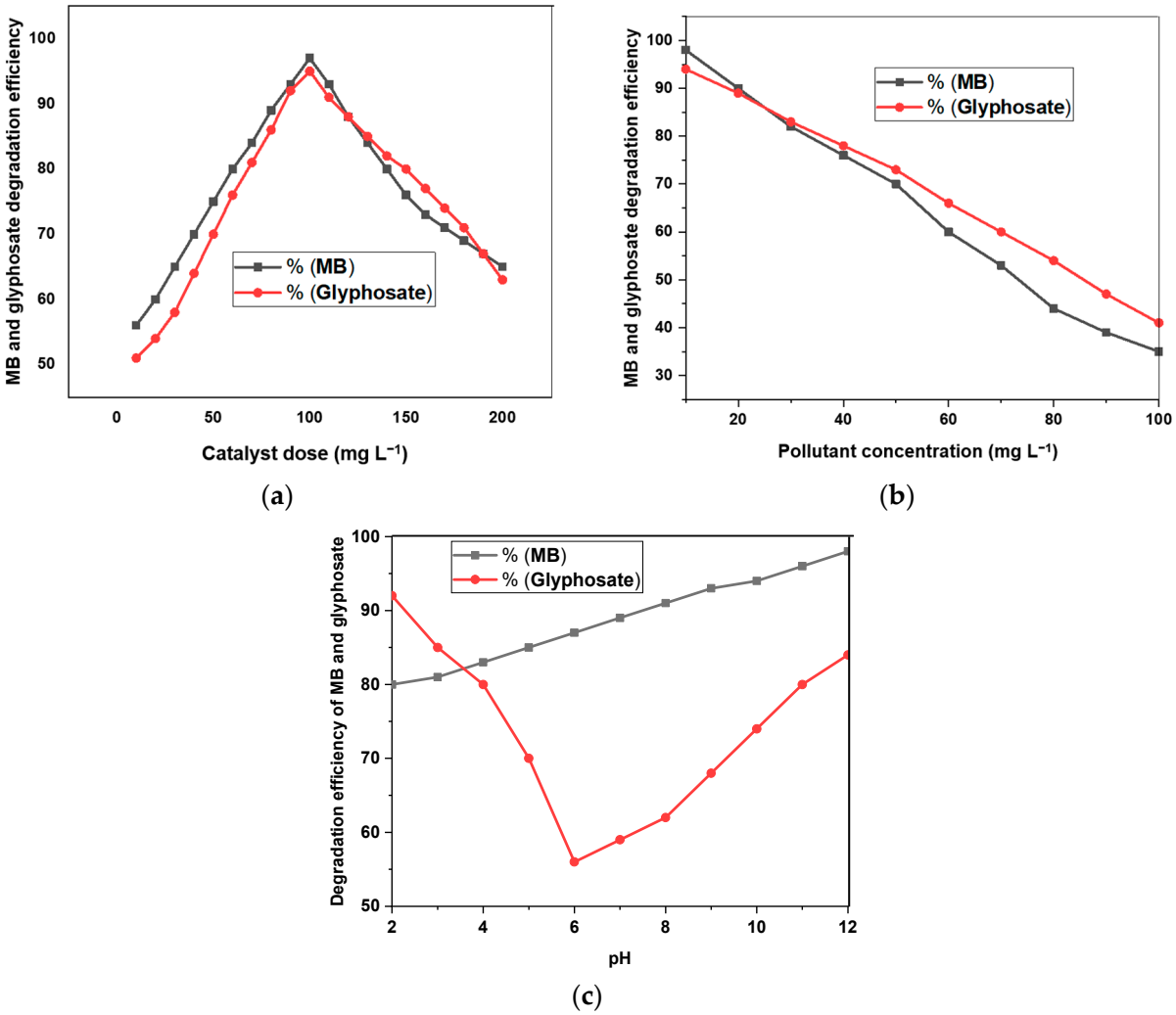


Figure 10. (**a**) DM g. C_3N_4-Ag-TiO_2 dosage effect on degradation efficiency of MB and glyphosate after 105 min. (**b**) MB and glyphosate concentration effect on degradation efficiency using DM g. C_3N_4-Ag-TiO_2 after 105 min. (**c**) pH effect on degradation of MB and glyphosate using DM g. C_3N_4-Ag-TiO_2 after 105 min.

2.9.2. Pollutant Concentration

The concentration of pollutants plays a vital role in determining the degradation efficiency of photocatalysts. The degradation efficiency was estimated by varying concentrations of MB and glyphosate from 10 mg L^{-1} to 100 mg L^{-1}. The MB degradation efficiency using DM g. C_3N_4-Ag-TiO_2 decreased from 98% to 35%, and the glyphosate degradation efficiency decreased from 94% to 41% with the increasing pollutant concentration at an optimum time of 105 min. The degradation efficiency for both MB and glyphosate indicated a decreasing trend with the increasing concentration of pollutants, as shown in Figure 10b. The absorption and intensity of light reaching the active sites of the surface decreased with the increasing pollutant concentration, leading to a decrease in the degradation efficiency, as reported in the literature [32].

2.9.3. pH Effect

The pH value varies in different water reservoirs and greatly affects the degradation efficiency of materials. The pH was varied from 2.0 to 12, and the degradation of MB and glyphosate was estimated for DM g. C_3N_4-Ag-TiO_2 at 105 min (Figure 10c). The MB degradation efficiency increased from 80% to 95% by varying the pH from 2.0 to 12. The degradation graph showed that the degradation of MB slightly increased with the increasing pH. The glyphosate degradation efficiency increased in both the acidic and basic mediums. When irradiated with light, the synthesized materials were excited to produce holes and electrons. These electrons and holes produced hydroxyl radicals used for the degradation of pollutants. In acidic conditions, the degradation of glyphosate is favored for Equations (4) and (5) (mentioned above). In basic conditions, the degradation process is favored for Equations (7) and (8) (mentioned above) [33]. In an acidic medium, the degradation is slightly higher compared to a basic medium. In the acidic medium, the maximum degradation efficiency of the photocatalyst for glyphosate was 92%, while in the basic medium, the maximum degradation efficiency of the catalyst for glyphosate was 84%.

2.10. Kinetic Study

A kinetic study of the photocatalytic process was performed by using the Langmuir–Hinshelwood model. The equilibrium absorption process was applied to study the degradation of persistent organic pollutants. The pseudo-first-order kinetics was investigated because the concentration of photocatalysts remains unchanged, while the concentration of pollutants decreases with time. A simplified form of Langmuir's expression for the pseudo-first-order can be given as follows:

$$\mathrm{Ln}\,(C_0 - C) = \mathrm{Ln}\,(C_0) - kt \quad (12)$$

In this equation, the initial concentration is C_0, while C indicates the concentration at any time, while k shows the rate constant for the pseudo-first-order reaction. The normalized concentration curves for MB and glyphosate degradation are shown in Figure 11a,b. (A), (B), (C), (D), and (E) in Figure 11a,b represent the photolytic, pure g. C_3N_4, DM g. C_3N_4, DM g. C_3N_4 decorated with silver, and the ternary composite of DM g. C_3N_4 decorated with Ag and TiO_2, respectively. The rate of oxidation or reduction of organic pollutants into simpler products depends upon the rate constant of the reaction [34]. The kinetics for the degradation of organic pollutants was studied for a time of 0–105 min. The values of the rate constant obtained by the slope for the different synthesized materials are listed in Table 2. The slope indicates that the rate constant for MB photodegradation was 0.03731 min^{-1} for DM g. C_3N_4-Ag-TiO_2 and 0.00006246 min^{-1} for the simple photolytic degradation of MB. The rate of photodegradation of MB using DM g. C_3N_4-Ag-TiO_2 was 597 times greater than the photolytic degradation. The half-life determined for the composite DM g. C_3N_4-Ag-TiO_2 was 18.72 min, while without using the catalyst, the half-life was 1117.74 min. The rate constant for the photodegradation of glyphosate using DM g. C_3N_4-Ag-TiO_2 was 0.00006486 min^{-1}, while the rate constant for the photolytic

degradation of glyphosate was 0.01589 min^{-1}. These results confirm that the photocatalysis followed pseudo-first-order kinetics for the degradation of organic pollutants into less hazardous products.

Table 2. Rate constant and half-life for degradation of MB and glyphosate by various nanoparticles and particle size obtained via XRD.

Sr. No.	Targeted Pollutant	Photocatalyst	Rate Constant (min^{-1})	Half-Life (min)
1	MB	Photolytic	0.00006246	11,095
2	MB	g. C_3N_4	0.00942	73.56
3	MB	DM g. C_3N_4	0.01213	57.13
4	MB	DM g. C_3N_4-Ag	0.01753	39.53
5	MB	DM g. C_3N_4-Ag-TiO_2	0.03731	18.57
6	Glyphosate	Photolytic	0.00006411	10,809
7	Glyphosate	g. C_3N_4	0.00446	155.38
8	Glyphosate	DM g. C_3N_4	0.00667	103.89
9	Glyphosate	DM g. C_3N_4-Ag	0.00906	76.49
10	Glyphosate	DM g. C_3N_4-Ag-TiO_2	0.01589	43.61

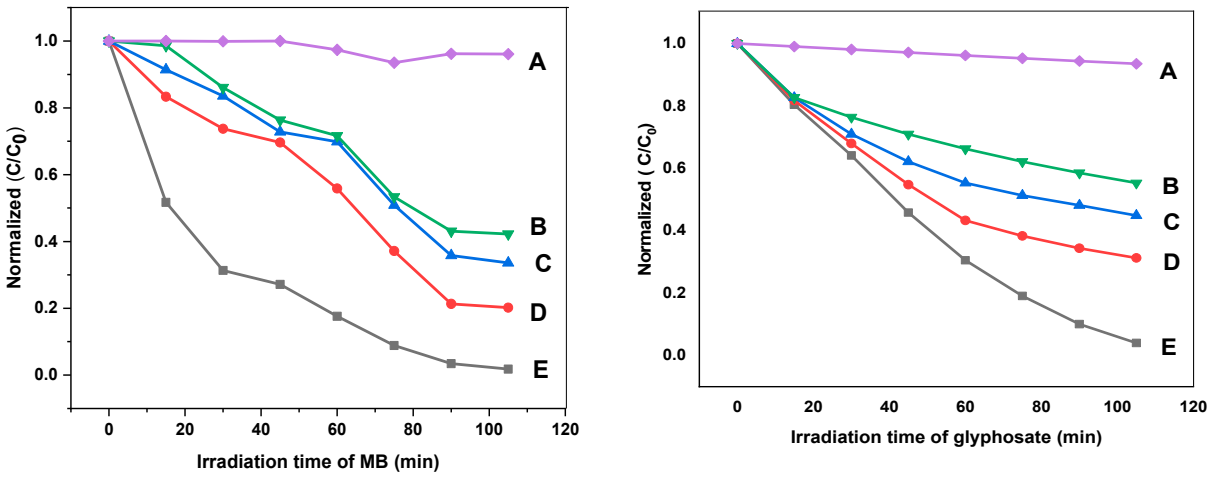


Figure 11. Normalized concentration curves for (**a**) MB degradation and (**b**) glyphosate degradation; A (photolytic), B (g. C_3N_4), C (DM g. C_3N_4), D (DM g. C_3N_4-Ag), E (DM g. C_3N_4-Ag-TiO_2).

2.11. Reusability/Stability of Catalysts

The stability of the prepared materials plays a vital role in their practical and long-time usage. The stability of DM g. C_3N_4-Ag-TiO_2 was studied by reusing the photocatalyst for the degradation of MB and glyphosate 10 times, and the results are shown in Figure 12. Every cycle of photocatalytic degradation of MB and glyphosate was studied for 105 min. After each degradation, the nanoparticles were recovered through centrifugation, washed with deionized water, and dried to use again. After ten cycles, the MB degradation efficiency slightly decreased from 97% to 80%, while the glyphosate degradation efficiency decreased from 96% to 79%. Reusing the photocatalysts for glyphosate and MB degradation multiple times confirmed that the surfaces of the catalysts mainly remained intact and stable with a slight decrease in the degradation efficiency. The XRD of DM g. C_3N_4-Ag-TiO_2 after 10 cycles of degradation of MB confirmed the presence of all the major peaks of the material, confirming the stability of the material (Figure 13). Moreover, the pollutant was not absorbed permanently on the surface of the synthesized material. The nanoparticles were easily separated from the pollutant via centrifugation. A decrease in the efficiency with the successive usage of the photocatalysts was thought to be due to the blockage of some active sites present on the surfaces of the photocatalysts [35].

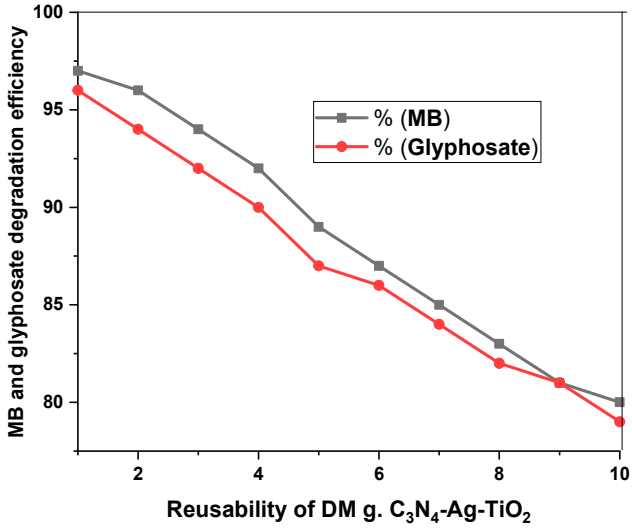


Figure 12. Effect of reusability of DM g. C_3N_4-Ag-TiO_2 for degradation of MB and glyphosate for 105 min.

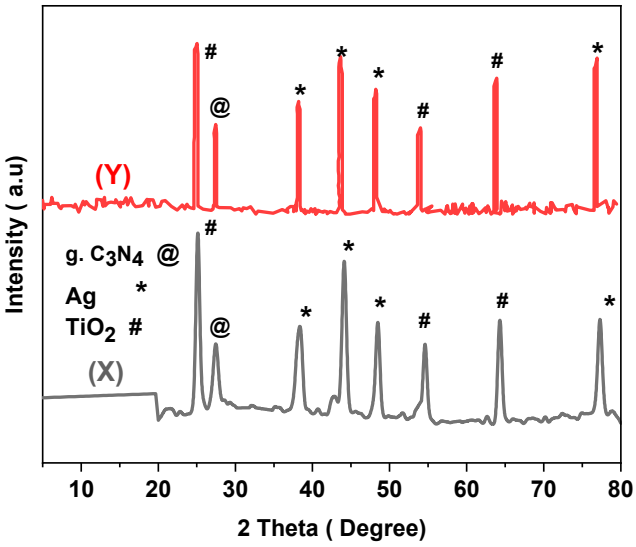


Figure 13. XRD of DM g. C_3N_4-Ag-TiO_2 (X) before degradation and (Y) after degradation of MB for 10 cycles.

2.12. Comparative Study between Various Nanoparticles for MB and Glyphosate Degradation

The use of various nanomaterials for the photocatalytic removal of glyphosate and MB was reported. A comparative analysis between the quantum yield (QY) and space–time yield (STY) (calculated by using Equations (13) and (14)) for the current study and previously reported materials was performed for MB and glyphosate removal (Table 3). The STY predicts the amount of pollutant degraded by the specific weight of the nanoparticles.

$$\text{QY} = \text{No.of molecules decayed s}^{-1}/\text{No.of photons s}^{-1} \quad (13)$$

$$\text{STY} = \text{QY}/\text{photocatalyst mass (mg)} \quad (14)$$

In the current study, a ternary composite of carbon nitride with silver and titanium oxide was investigated. A comparison was made between the current study and previously reported nanoparticles of silver, titanium oxide, and carbon nitride for the photocatalytic removal of glyphosate and MB.

Table 3. Comparison of degradation efficiency and quantum yield of current material with previously reported carbon nitride, silver, and titanium oxide materials.

Absorbent	Targeted Pollutants	Light Source	Catalyst Dosage (g)	Reaction Time (min)	Lamp Power (W)	Pollutant Concentration g L^{-1}	Removal Efficiency (%)	Quantum Yield Molecule $Photon^{-1}$	Space–Time Yield	Reference
Ag-ZnO	MB	UV	0.3	60	6	0.01	87.74	1.1×10^{-6}	3.8×10^{-8}	[36]
Ag-TiO_2	MB	UV	1	120	15	0.057	80.33	1.6×10^{-5}	1.6×10^{-8}	[32]
CaO-loaded 3D g. C_3N_4	MB	UV	0.2	15	20	0.01	99	1.8×10^{-5}	9.3×10^{-8}	[32]
Metal-free g. C_3N_4	MB	Visible	0.1	180	80	0.01	81	5.3×10^{-7}	5.3×10^{-9}	[37]
DM g. C_3N_4-Ag-TiO_2	MB	Visible	0.1	105	40	0.1	98	5.7×10^{-6}	5.7×10^{-8}	Current study
Boron-doped diamond/Tio_2	Glyphosate	UV	0.2	300	9	0.05	95.2	7.9×10^{-6}	4.0×10^{-7}	[38]
Cyclodextrin MoS_2-g. C_3N_4	Glyphosate	Visible	0.2	180	300	0.9	79	4.9×10^{-4}	2.4×10^{-5}	[39]
β-CD/g. C_3N_4-MoS_2	Glyphosate	Visible	0.2	180	300	9	80	1.2×10^{-4}	5.9×10^{-6}	[40]
$BiVO_4$-g. C_3N_4	Glyphosate	Visible	.08	150	125	0.1	69	8.3×10^{-6}	1.0×10^{-7}	[41]
DM g. C_3N_4-Ag-TiO_2	Glyphosate	Visible	0.1	105	40	0.1	97	2.8×10^{-5}	2.8×10^{-7}	Current study

3. Experimental Procedure

3.1. Materials

Analytical-grade methylene blue (99%), glyphosate (96%), barium carbonate (99.99%), thiourea (99%), DMF (99.8%), silver nitrate (99%), titanium isopropoxide (97%), and ethylene glycol (99.8%) were obtained from Merck (Darmstadt, Germany). All the precursors and chemicals were applied without any treatment. Hydrochloric acid (percentage 36.5–38%) obtained from Merck was used for washing purposes.

3.2. Synthesis of Pristine and Barium Defect-Modified g. C_3N_4

Pure g. C_3N_4 was synthesized by using thiourea precursor. Typically, a 5 g thiourea is put in a vacuum desiccator for 24 h to ensure the purity of the precursor. This purified precursor was taken in the crucible and calcinated in a furnace at 610 °C for 2 h to obtain g. C_3N_4. The DM g. C_3N_4 was prepared by using barium carbonate and thiourea precursor in a 1:4 ratio. For homogenous mixing, both precursors were poured into 10 mL of deionized water (DI) and sonicated for an hour. Then, overnight drying of the mixture in the oven was performed at 70 °C. Calcination of material was performed in a furnace for 2 h at 610 °C. The product obtained was washed with hydrochloric acid and water three times [42].

3.3. Synthesis of DM g. C_3N_4 Decorated with Ag and TiO_2

A total of 10 mg DM g. C_3N_4 was dried overnight in a vacuum desiccator for purification purposes. A total of 30 mL dimethylformamide (DMF) was added to it, and sonication was performed for 1 h at 30 °C. Then, 100 mg silver nitrate and 10 mL ethylene glycol were added to it, followed by sonication and stirring to homogenize the mixture. After the addition of 1.3 mL of titanium isopropoxide, the mixture was transferred to an autoclave. Then, the autoclave was kept in the heating oven at 185 °C for 24 h. Washing of greyish products was performed by using ethanol and deionized water [43,44].

3.4. Characterization of Photocatalysts

Functional elucidation of various synthesized materials was performed using SHIMADZU-IR PRESTIGE-2 spectrophotometer (Kyoto, Tapan). Samples were excited by using a pulsed laser at 10 Hz. Fast detection was performed using a fast MCT detector containing mercury, cadmium, and a telluride detector, which helped to obtain the resolution at a time of up to 2.5 nanoseconds. Signal-to-noise ratio was improved by performing all the measurements under vacuum conditions. An amount of 2 mg of sample in 200 mg KBr was pressed to a KBr pallet to record the spectrum [45]. X-ray diffraction was used for phase determination of the synthesized materials. Powdered XRD of the materials using D 8 diffractometer (Bruker, Germany) equipped with Cu Kαradiation (α= 1.5418 Å) provided information about the structure and nature of the crystals, while the phase of the polycrystalline materials and lattice parameters were also investigated via XRD. Lattice parameters were calculated by using the following formula.

$$a = d(h^2 + k^2 + l^2)^{1/2} \quad (15)$$

In Equation (15) "a" indicates the length of the unit cell, "d" is the lattice plane distance, and h^2, k^2, and l^2 represent miller indices.

The average particle size of prepared materials was calculated using the Debye–Scherrer formula.

$$D = k\lambda / \beta \, \mathrm{Cos}\theta \quad (16)$$

"D" indicates particle size, "K" is Scherrer constant, λ is the wavelength of the X-ray, and β shows the full width at half maximum of the diffraction peak in Equation (16).

The morphology of the prepared materials was confirmed using SEM analysis. JEOL EDS system (Tokyo, Japan) was used to study the number of elements and their atomic percentage in the composite. The optical properties of the base material and other prepared materials were estimated by using a Shimadzu-1800 UV/Visible spectrophotometer (Kyoto, Tapan). Photocatalytic degradation of organic pollutants occurs due to different

active species. These species mainly involve hydroxyl radicals, free electrons, holes, and superoxide radicals. Trapping experiments by using different scavengers were performed to study the role of active species in the photodegradation process. Scavenger analysis helped in finding the possible mechanism for the photocatalytic degradation of pollutants.

3.5. Degradation Study and Optimization of Various Experimental Conditions

A Philips 40-watt visible light bulb (Amsterdam, the Netherlands) was used as a solar light irradiation source to carry out the degradation study of the pollutants via nanoparticles in a photoreactor. The absorption efficiency of prepared nanoparticles for the degradation of pollutants was evaluated by recording the UV/Visible spectrum of the liquid samples. For each calculation, an appropriate amount of synthesized material was put in an aqueous solution of dye or pesticide. The sample was stirred in the dark for 30 min to obtain equilibrium. After homogenization was achieved, C_0 was calculated by drawing a 15 mL sample and recording UV/Visible absorption spectra. Then, the sample was irradiated with a light source while keeping the stirring on. After every 15 min, a sample was drawn and centrifuged, and the absorption spectrum was recorded by using the same procedure. Results confirm that complete degradation of MB and glyphosate was achieved in 105 min. For comparison, simple photolytic degradation spectra of MB and glyphosate were also recorded without the addition of a catalyst. UV/Visible degradation spectra for MB and glyphosate were recorded for simple carbon nitride, defect-modified graphitic carbon nitride, silver-decorated defect-modified carbon nitride, and the ternary composite of silver and titanium oxide with defect-modified carbon nitride. Degradation efficiency was estimated by using the following equation [46].

$$\% \text{ Degradation of pollutant} = \frac{C_0 - C}{C_0} \times 100 \quad (17)$$

C_0 is UV/Vis absorption value of the sample before light irradiation. C is the value of absorption at any given time. Absorption values were calculated by using lambda max (λ_{max}) 664 nm and 260 nm for MB and glyphosate, respectively. Different parameters such as the pH effect, catalyst dose effect, the concentration of pollutants, stability of the catalyst, etc., were studied and optimized by using an absorption study [47]. The stability of the synthesized nanocomposite was performed via regeneration study. A kinetic study was performed by applying the Langmuir–Hinshelwood model.

4. Conclusions

Carbon nitride is considered an important base material for efficient photocatalytic activity. In our work, barium defect-modified carbon nitride was used as the base material. The ternary composite was prepared by decorating the base material with silver and titanium oxide. The prepared composite showed excellent efficiency in the removal of glyphosate and MB from water. A series of structural characterizations were applied to confirm the efficient synthesis of the composite and other photocatalysts. The photocatalytic degradation results were obtained by taking the UV/Visible absorption spectra. The absorbance values were measured at characteristic wavelengths of 664 nm and 260 nm for MB and glyphosate, respectively. Decorating carbon nitride with silver and titanium oxide increased the visible light response by increasing both the VB and CB response. With the introduction of TiO_2 and silver, the recombination rate of the holes and electrons was lowered, and as a result, more photogenerated electrons and holes were produced. The lowering of the recombination rate was confirmed by a decrease in the intensity of the photoluminescence spectrum. Glyphosate and MB were almost completely degraded by DM g. C_3N_4-Ag-TiO_2 after one hour and forty-five minutes. The XRD analysis of the DM g. C_3N_4-Ag-TiO_2 after ten cycles of photocatalytic degradation of MB showed persistence of all the major peaks of the material. After using the catalyst ten times, the structure of the composite mainly remained intact, confirming the higher stability of the prepared material. These results confirm the efficient removal of pollutants from water resources using synthesized materials.

Author Contributions: K.A., experiments and original draft; A.N., supervision, review and editing; S.M., M.I.K., J.F.G. and A.S., software, validation, resources, review, and formatting. All authors have read and agreed to the published version of the manuscript.

Funding: The authors would like to acknowledge the financial support from the Office of Research, Innovation, and Commercialization (ORIC) at Bahauddin Zakariya University, Multan (BZU); the Higher Education Commission collaborative program within the project COL-PD-2019.45897; and the IQS-School of Engineering considering the consolidated research group 2021 SGR 00321.

Data Availability Statement: The complete data are presented in the manuscript.

Conflicts of Interest: The authors declare that they have no known competing financial interest or personal relationships that could have appeared to influence the work reported in this paper.

References

1. Akpan, U.G.; Hameed, B.H. Parameters affecting the photocatalytic degradation of dyes using TiO_2-based photocatalysts: A review. *J. Hazard. Mater.* **2009**, *170*, 520–529. [CrossRef] [PubMed]
2. Rauf, M.; Ashraf, S.S. Fundamental principles and application of heterogeneous photocatalytic degradation of dyes in solution. *Chem. Eng. J.* **2009**, *151*, 10–18. [CrossRef]
3. Reza, K.M.; Kurny, A.; Gulshan, F. Parameters affecting the photocatalytic degradation of dyes using TiO_2: A review. *Appl. Water Sci.* **2017**, *7*, 1569–1578. [CrossRef]
4. Tanaka, K.; Padermpole, K.; Hisanaga, T. Photocatalytic degradation of commercial azo dyes. *Water Res.* **2000**, *34*, 327–333. [CrossRef]
5. Gregory, P. Classification of dyes by chemical structure. In *The Chemistry and Application of Dyes*; Waring, D.R., Hallas, G., Eds.; Springer: New York, NY, USA, 1990; pp. 17–47.
6. Houas, A.; Lachheb, H.; Ksibi, M.; Elaloui, E.; Guillard, C.; Herrmann, J.-M. Photocatalytic degradation pathway of methylene blue in water. *Appl. Catal. B Environ.* **2001**, *31*, 145–157. [CrossRef]
7. Pizzul, L.; Castillo, M.d.P.; Stenström, J. Degradation of glyphosate and other pesticides by ligninolytic enzymes. *Biodegradation* **2009**, *20*, 751–759. [CrossRef]
8. Dick, R.; Quinn, J. Glyphosate-degrading isolates from environmental samples: Occurrence and pathways of degradation. *Appl. Microbiol. Biotechnol.* **1995**, *43*, 545–550. [CrossRef]
9. Lewis, K.A.; Tzilivakis, J.; Warner, D.J.; Green, A. An international database for pesticide risk assessments and management. *Hum. Ecol. Risk Assess. Int. J.* **2016**, *22*, 1050–1064. [CrossRef]
10. Viswanathan, B. Photocatalytic degradation of dyes: An overview. *Curr. Catal.* **2018**, *7*, 99–121. [CrossRef]
11. Chen, F.; Xie, Y.; Zhao, J.; Lu, G. Photocatalytic degradation of dyes on a magnetically separated photocatalyst under visible and UV irradiation. *Chemosphere* **2001**, *44*, 1159–1168. [CrossRef]
12. Nagaveni, K.; Sivalingam, G.; Hegde, M.; Madras, G. Solar photocatalytic degradation of dyes: High activity of combustion synthesized nano TiO_2. *Appl. Catal. B Environ.* **2004**, *48*, 83–93. [CrossRef]
13. Rupa, A.V.; Manikandan, D.; Divakar, D.; Sivakumar, T. Effect of deposition of Ag on TiO_2 nanoparticles on the photodegradation of Reactive Yellow-17. *J. Hazard. Mater.* **2007**, *147*, 906–913. [CrossRef]
14. Bhatia, S.; Verma, N.; Bedi, R. Optical application of Er-doped ZnO nanoparticles for photodegradation of direct red-31 dye. *Opt. Mater.* **2016**, *62*, 392–398. [CrossRef]
15. Vasiliev, V.V.; Morozov, E.V. *Mechanics and Analysis of Composite Materials*; Elsevier: Amsterdam, The Netherlands, 2001.
16. Manzoor, S.; Garcia, J.F.; Shah, K.H.; Khan, M.I.; Abbas, N.; Raza, H.; Mubarik, S.; Hayat, M.; Iram, A.; Yar, A. Multipollutant Abatement through Visible Photocatalytic System. *Catalysts* **2023**, *13*, 65. [CrossRef]
17. Naseem, K.; Tahir, M.H.; Farooqi, F.; Manzoor, S.; Khan, S.U. Strategies adopted for the preparation of sodium alginate–based nanocomposites and their role as catalytic, antibacterial, and antifungal agents. *Rev. Chem. Eng.* **2022**. [CrossRef]
18. Koe, W.S.; Lee, J.W.; Chong, W.C.; Pang, Y.L.; Sim, L.C. An overview of photocatalytic degradation: Photocatalysts, mechanisms, and development of photocatalytic membrane. *Environ. Sci. Pollut. Res.* **2020**, *27*, 2522–2565. [CrossRef]
19. Sun, X.; Yan, L.; Xu, R.; Xu, M.; Zhu, Y. Surface modification of TiO_2 with polydopamine and its effect on photocatalytic degradation mechanism. *Colloids Surf. A Physicochem. Eng. Asp.* **2019**, *570*, 199–209. [CrossRef]
20. Sudhaik, A.; Raizada, P.; Shandilya, P.; Jeong, D.-Y.; Lim, J.-H.; Singh, P. Review on fabrication of graphitic carbon nitride based efficient nanocomposites for photodegradation of aqueous phase organic pollutants. *J. Ind. Eng. Chem.* **2018**, *67*, 28–51. [CrossRef]
21. Katsumata, K.-i.; Motoyoshi, R.; Matsushita, N.; Okada, K. Preparation of graphitic carbon nitride (g-C_3N_4)/WO_3 composites and enhanced visible-light-driven photodegradation of acetaldehyde gas. *J. Hazard. Mater.* **2013**, *260*, 475–482. [CrossRef] [PubMed]
22. Niu, P.; Liu, G.; Cheng, H.-M. Nitrogen vacancy-promoted photocatalytic activity of graphitic carbon nitride. *J. Phys. Chem. C* **2012**, *116*, 11013–11018. [CrossRef]
23. Sun, M.; Fang, Y.; Kong, Y.; Sun, S.; Yu, Z.; Umar, A. Graphitic carbon nitride (g-C_3N_4) coated titanium oxide nanotube arrays with enhanced photo-electrochemical performance. *Dalton Trans.* **2016**, *45*, 12702–12709. [CrossRef]

24. Wang, L.; Wang, C.; Hu, X.; Xue, H.; Pang, H. Metal/graphitic carbon nitride composites: Synthesis, structures, and applications. *Chem. Asian J.* **2016**, *11*, 3305–3328. [CrossRef] [PubMed]
25. Abdullahi, S.S.; Güner, S.; Musa, Y.; Adamu, B.I.; Abdulhamid, M.I. Sımple method for the determınatıon of band gap of a nanopowdered sample usıng Kubelka Munk theory. *NAMP J.* **2016**, *35*, 241–246.
26. López, R.; Gómez, R. Band-gap energy estimation from diffuse reflectance measurements on sol–gel and commercial TiO_2: A comparative study. *J. Sol-Gel Sci. Technol.* **2012**, *61*, 1–7. [CrossRef]
27. Nasuha, N.; Ismail, S.; Hameed, B. Activated electric arc furnace slag as an effective and reusable Fenton-like catalyst for the photodegradation of methylene blue and acid blue 29. *J. Environ. Manag.* **2017**, *196*, 323–329. [CrossRef] [PubMed]
28. Moosavi, S.; Li, R.Y.M.; Lai, C.W.; Yusof, Y.; Gan, S.; Akbarzadeh, O.; Chowhury, Z.Z.; Yue, X.-G.; Johan, M.R. Methylene blue dye photocatalytic degradation over synthesised Fe_3O_4/AC/TiO_2 nano-catalyst: Degradation and reusability studies. *Nanomaterials* **2020**, *10*, 2360. [CrossRef]
29. Silva, J.; Neto, N.A.; Teodoro, M.; Paiva, A.; Bomio, M.; Motta, F. Fabrication of new Ag_2CrO_4/Ag_2MoO_4 and Ag_2CrO_4/Ag_2WO_4 heterostructures with enhanced degradation of the mixture of dyes by photocatalysis. *J. Alloys Compd.* **2022**, *928*, 167136. [CrossRef]
30. Zhu, C.; Wang, L.; Kong, L.; Yang, X.; Wang, L.; Zheng, S.; Chen, F.; MaiZhi, F.; Zong, H. Photocatalytic degradation of AZO dyes by supported TiO_2 + UV in aqueous solution. *Chemosphere* **2000**, *41*, 303–309. [CrossRef] [PubMed]
31. Kong, J.-Z.; Li, A.-D.; Li, X.-Y.; Zhai, H.-F.; Zhang, W.-Q.; Gong, Y.-P.; Li, H.; Wu, D. Photo-degradation of methylene blue using Ta-doped ZnO nanoparticle. *J. Solid State Chem.* **2010**, *183*, 1359–1364. [CrossRef]
32. Sahoo, C.; Gupta, A. Optimization of photocatalytic degradation of methyl blue using silver ion doped titanium dioxide by combination of experimental design and response surface approach. *J. Hazard. Mater.* **2012**, *215*, 302–310. [CrossRef]
33. Alkaim, A.; Aljeboree, A.; Alrazaq, N.; Baqir, S.; Hussein, F.; Lilo, A. Effect of pH on adsorption and photocatalytic degradation efficiency of different catalysts on removal of methylene blue. *Asian J. Chem.* **2014**, *26*, 8445. [CrossRef]
34. Fan, H.; Zhao, X.; Yang, J.; Shan, X.; Yang, L.; Zhang, Y.; Li, X.; Gao, M. ZnO–graphene composite for photocatalytic degradation of methylene blue dye. *Catal. Commun.* **2012**, *29*, 29–34. [CrossRef]
35. Saeed, M.; Muneer, M.; Akram, N.; ul Haq, A.; Afzal, N.; Hamayun, M. Synthesis and characterization of silver loaded alumina and evaluation of its photo catalytic activity on photo degradation of methylene blue dye. *Chem. Eng. Res. Des.* **2019**, *148*, 218–226. [CrossRef]
36. Rafaie, H.; Nor, R.; Azmina, M.; Ramli, N.; Mohamed, R. Decoration of ZnO microstructures with Ag nanoparticles enhanced the catalytic photodegradation of methylene blue dye. *J. Environ. Chem. Eng.* **2017**, *5*, 3963–3972. [CrossRef]
37. Song, L.; Zhang, S.; Wu, X.; Wei, Q. A metal-free and graphitic carbon nitride sonocatalyst with high sonocatalytic activity for degradation methylene blue. *Chem. Eng. J.* **2012**, *184*, 256–260. [CrossRef]
38. Alulema-Pullupaxi, P.; Fernández, L.; Debut, A.; Santacruz, C.P.; Villacis, W.; Fierro, C.; Espinoza-Montero, P.J. Photoelectrocatalytic degradation of glyphosate on titanium dioxide synthesized by sol-gel/spin-coating on boron doped diamond (TiO_2/BDD) as a photoanode. *Chemosphere* **2021**, *278*, 130488. [CrossRef]
39. Wu, Z.; He, X.; Xue, Y.; Yang, X.; Li, Y.; Li, Q.; Yu, B. Cyclodextrins grafted MoS_2/g-C_3N_4 as high-performance photocatalysts for the removal of glyphosate and Cr (VI) from simulated agricultural runoff. *Chem. Eng. J.* **2020**, *399*, 125747. [CrossRef]
40. He, X.; Wu, Z.; Xue, Y.; Gao, Z.; Yang, X. Fabrication of interlayer β-CD/g-C_3N_4@MoS_2 for highly enhanced photodegradation of glyphosate under simulated sunlight irradiation. *RSC Adv.* **2019**, *9*, 4635–4643. [CrossRef] [PubMed]
41. Huo, R.; Yang, X.-L.; Yang, J.-Y.; Yang, S.-Y.; Xu, Y.-H. Self-assembly synthesis of $BiVO_4$/Polydopamine/g-C_3N_4 with enhanced visible light photocatalytic performance. *Mater. Res. Bull.* **2018**, *98*, 225–230. [CrossRef]
42. Li, K.; Jiang, Y.; Li, Y.; Wang, Z.; Liu, X.; Wang, P.; Xia, D.; Fan, R.; Lin, K.; Yang, Y. In situ preparation of graphitic carbon nitride bonded with cyano groups for enhanced photocatalytic activity. *Int. J. Hydrogen Energy* **2020**, *45*, 9683–9694. [CrossRef]
43. Paul, D.R.; Sharma, R.; Panchal, P.; Nehra, S.; Gupta, A.; Sharma, A. Synthesis, characterization and application of silver doped graphitic carbon nitride as photocatalyst towards visible light photocatalytic hydrogen evolution. *Int. J. Hydrogen Energy* **2020**, *45*, 23937–23946. [CrossRef]
44. Jiang, Z.; Liu, D.; Jiang, D.; Wei, W.; Qian, K.; Chen, M.; Xie, J. Bamboo leaf-assisted formation of carbon/nitrogen co-doped anatase TiO_2 modified with silver and graphitic carbon nitride: Novel and green synthesis and cooperative photocatalytic activity. *Dalton Trans.* **2014**, *43*, 13792–13802. [CrossRef] [PubMed]
45. Tichapondwa, S.M.; Newman, J.; Kubheka, O. Effect of TiO_2 phase on the photocatalytic degradation of methylene blue dye. *Phys. Chem. Earth Parts A/B/C* **2020**, *118*, 102900. [CrossRef]
46. Neppolian, B.; Choi, H.; Sakthivel, S.; Arabindoo, B.; Murugesan, V. Solar/UV-induced photocatalytic degradation of three commercial textile dyes. *J. Hazard. Mater.* **2002**, *89*, 303–317. [CrossRef]
47. Wang, Q.; Chen, C.; Zhao, D.; Ma, W.; Zhao, J. Change of adsorption modes of dyes on fluorinated TiO_2 and its effect on photocatalytic degradation of dyes under visible irradiation. *Langmuir* **2008**, *24*, 7338–7345. [CrossRef]

Disclaimer/Publisher's Note: The statements, opinions and data contained in all publications are solely those of the individual author(s) and contributor(s) and not of MDPI and/or the editor(s). MDPI and/or the editor(s) disclaim responsibility for any injury to people or property resulting from any ideas, methods, instructions or products referred to in the content.